Hybrid Monte Carlo and continuum modeling of electrolytes with concentration-induced dielectric variations

Xiaofei Guan,[1,*] Manman Ma,[2,†] Zecheng Gan,[3,‡] Zhenli Xu,[4,§] and Bo Li[5,‖]

[1]*School of Mathematical Sciences, Tongji University, 1239 Siping Road, Shanghai, 200092, China*

[2]*School of Mathematical Sciences and Institute of Natural Sciences, Shanghai Jiao Tong University, Shanghai 200240, China*

[3]*Department of Mathematics, University of Michigan, Ann Arbor, Michigan 48109, USA*

[4]*School of Mathematical Sciences, Institute of Natural Sciences, and MoE Key Lab of Scientific and Engineering Computing, Shanghai Jiao Tong University, Shanghai 200240, China*

[5]*Department of Mathematics and Graduate Program in Quantitative Biology, University of California, San Diego, California 92093-0112, USA*

The distribution of ions near a charged surface is an important quantity in many biological and material processes, and has been therefore investigated intensively. However, few theoretical and simulation approaches have included the influence of concentration-induced variations in the local dielectric permittivity of an underlying electrolyte solution. Such local variations have long been observed and known to affect the properties of ionic solution in the bulk and around the charged surface. We propose a hybrid computational model that combines Monte Carlo simulations with continuum electrostatic modeling to investigate such properties. A key component in our hybrid model is a semianalytical formula for the ion-ion interaction energy in a dielectrically inhomogeneous environment. This formula is obtained by solving for the Green's function Poisson's equation with ionic-concentration-dependent dielectric permittivity using a harmonic interpolation method and spherical harmonic series. We also construct a self-consistent continuum model of electrostatics to describe the effect of ionic-concentration-dependent dielectric permittivity and the resulting self-energy contribution. With extensive numerical simulations, we verify the convergence of our hybrid simulation scheme, show the qualitatively different structures of ionic distribution due to the concentration-induced dielectric variations, and compare our simulation results with the self-consistent continuum model. In particular, we study the differences between weakly and strongly charged surfaces and multivalencies of counterions. Our hybrid simulations conform particularly the depletion of ionic concentrations near a charged surface and also capture the charge inversion. We discuss several issues and possible further improvement of our approach for simulations of large charged systems.

I. INTRODUCTION

The formation and structure of an electric double layer (EDL) around a charged colloid immersed in an electrolyte solution is largely determined by a high gradient of the electric potential around the colloid. Such electric potential is determined by fixed charges (e.g., surface charges), charges of ions, and the solvent polarization. The distribution of ions near the colloidal surface therefore characterizes EDL structures. An EDL has a significant influence on the behavior of microscopic and mesoscopic charged particles that are in contact with solution. Understanding ionic distributions near a charged surface and hence the structure of EDL is therefore crucial to many applications, including energy-saving devices, membranes, and biopolymers [1–3].

Computationally, all-atom simulations of mesoscopic systems are prohibitively expensive because of the repeated energy or force evaluations for a system with large number of particles. Alternative continuum approximations and coarse-grained models are rather efficient, and the classical Poisson-Boltzmann (PB) theory [4–6] is a representative continuum model of such efficient approaches. While this simple and effective theory has been quite successful in predicting some basic properties of an EDL structure, it is known to be only accurate in the weak-coupling regime and with low ionic concentrations. For instance, the PB theory is unable to describe the ionic depletion near an air-electrolyte interface, as well as over charging, charge reversal, stratification of ionic concentrations, and ion-mediated like-charge attractions [7–15]. It is believed that the main reason for the PB theory to be quite restrictive is that it does not describe well the many-body correlations.

A different and also widely used coarse-grained computational model is the primitive model [16,17]. In such a model, the solvent (e.g., water) molecules, often of very large numbers, are treated implicitly and collectively as a continuum medium with a spatially homogeneous dielectric constant. Mobile ions, however, are still explicitly treated as discrete, charged particles. As the dielectric environment is in general nonuniform, its approximation with a dielectric constant can lead naturally to an issue of the dielectric effect. In fact, the dielectric polarization effect has been found to play an important role in a variety of systems, such as colloid suspensions [18–21], cloud droplets [22,23], and protein folding [24]. In order to investigate such a polarization effect with the primitive model, one needs to account for the effect of dielectric mismatch across an interface, the

———————

[*]guanxf@tongji.edu.cn

[†]mmm@sjtu.edu.cn

[‡]zecheng@umich.edu

[§]xuzl@sjtu.edu.cn

[‖]bli@math.ucsd.edu

dielectric boundary, from a low dielectric material to the high dielectric aqueous solvent. This can be done by solving Poisson's equation or Poisson-Boltzmann equation for the electrostatic potential with a spatially piecewise constant dielectric coefficient.

Computer simulation studies with the primitive model and dielectric boundary Poisson's model with piecewise dielectric coefficient have confirmed that the dielectric boundary does have a significant influence on many-body phenomena, such as charge inversion, like-charge attraction, and electrostatics-driven colloidal self-assembly [21,25–28]. Such an approach, however, still has some obvious drawbacks. First, numerically solving such dielectric boundary Poisson's equation for arbitrary geometries can be rather expensive, unless the underlying system geometry is simple (e.g., a spherical interface) and a corresponding efficient method (such as the image charge method) is used [27]. In recent years, several efficient techniques for general system geometries have been developed. These include the induced charge computation method [29–31], boundary element method [32], energy functional approaches [33,34], and the local electrostatic method based on the Maxwell equations [35]. However, the efficiency is still an issue, particularly when such a method is combined with Monte Carlo (MC) or molecular dynamics (MD) simulations. Second, a more serious issue is that the dielectric description is still far from reality. For instance, the dielectric fluctuation effect due to the alignment of ordered dipoles is ignored in these descriptions. Experimentally, the solvent itself can be polarized, leading to its effective dielectric permittivity being spatially varying as a function of the salt concentration [36,37]. Heuristically, salt ions weaken the ability of the realignment of solvent molecules with an applied field. Thus, a locally high salt concentration effectively decreases the dielectric permittivity in that region. This effect has been less studied, mostly due to the difficulty in efficiently solving Poisson's equation with a spatially varying coefficient coupled with particle based simulations.

In this work, we develop a hybrid MC simulations and continuum electrostatics model to study an electrolyte solution. This model allows us to self-consistently calculate the equilibrium ionic distributions in a medium with salt-concentration-dependent local dielectric permittivity. We describe this local dielectric permittivity by an analytic formula that fits experimental data and all-atom MD simulation results [38,39]. We combine the MC simulation scheme with a harmonic interpolation method (HIM) [40] for rapidly solving Poisson's equation with spatially varying dielectric coefficient. We also construct a self-consistent continuum model (SCCM) that extends a previous model developed in [41,42]. This model is in the form of Poisson's equation together with generalized Boltzmann distributions that account for self-energies. We develop various efficient numerical methods to implement our model. These include an approximation method using a homogeneous dielectric permittivity and a method of line image charge [43].

After we verify the convergence of our computational methods, we apply them to investigate the effect of ionic-concentration-dependent dielectric permittivity to the EDL structure around a charged colloidal particle. In particular, we consider both low and high charge densities of the colloidal surface, as well as multivalencies of counterions in the electrolyte solution. Moreover, we compare our hybrid MC simulation results with standard MC simulation results in which a constant dielectric coefficient in the region of electrolyte is used. We also compare our hybrid MC simulation results with those obtained from calculations based on our self-consistent continuum model. Our extensive computations demonstrate the attractive performance of our method and reveal several interesting phenomena arising from the ionic-concentration-induced variations in the dielectric permittivity.

We organize the rest of our paper as follows. In Sec. II, we describe our hybrid MC simulations and continuum electrostatics model and provide details of the harmonic interpolation method (HIM) for solving the continuum electrostatics problem coupled in MC simulations. In Sec. III, we introduce the self-consistent continuum model and our method of implementation for this model. In Sec. IV, we report simulation results with discussions. Finally, in Sec. V, we draw conclusions and discuss some issues and possible improvement of our approaches.

II. A HYBRID MONTE CARLO SIMULATIONS AND CONTINUUM ELECTROSTATICS MODEL

We propose a canonical-ensemble Metropolis Monte Carlo (MC) method for an extended primitive model that accounts for the dielectric inhomogeneity arising from the dependence of the dielectric coefficient on local, total ionic concentration. By fitting experimental and simulations data [44,45], we obtain the following formula of the dielectric coefficient (i.e., relative permittivity) varying with the total ionic concentration [38]:

$$\varepsilon(c) = 70e^{-0.22c/c_0} + 10, \tag{1}$$

where $c = \sum_{j=1}^{M} c_j$ with M the number of species of ions and c_j the local concentration of the jth ionic species, and $c_0 = 1$ M. In Eq. (1), we have implicitly assumed that the dielectric coefficient ε_{w} (w for water) for the pure solvent (i.e., $c = 0$) is $\varepsilon_{\mathrm{w}} = \varepsilon(0) = 80$.

A. The Hamiltonian

We consider a negatively charged colloidal particle immersed in an electrolyte solution (cf. Fig. 1). (There is no particular reason, other than being specific, for us to consider a negatively charged macroion.) The macroion is centered at $\mathbf{r}_0 = \mathbf{O}$ (the origin), has radius R_{m}, and has a bare charge $Q_0 = Z_0 e$ at its center, where Z_0 is the valence and e is the elementary charge. The electrolyte solution occupies a spherical shell defined by $R_{\mathrm{m}} < r < R_{\mathrm{shell}}$ for some radius R_{shell}, where $r = |\mathbf{r}|$ [17]. We assume that there are N microions of M different ionic species in the electrolyte solution. The ith ion is located at $\mathbf{r}_i$ (the center of ion), has radius a_i, and carries a charge $q_i = z_i e$ at its center with z_i its valence. An ion of jth species has valence Z_j. So, each $z_i (1 \leqslant i \leqslant N)$ is the same as some Z_j $(1 \leqslant j \leqslant M)$. We also assume that the entire charged system satisfies the electroneutrality condition. With a given set of microions, we define the ionic concentrations $c_j = c_j(\mathbf{r})$ $(j = 1, \ldots, M)$ and the total concentration $c(\mathbf{r}) = \sum_{j=1}^{M} c_j(\mathbf{r})$. With our underlying system geometry, we shall assume that all these concentrations are radially symmetric,
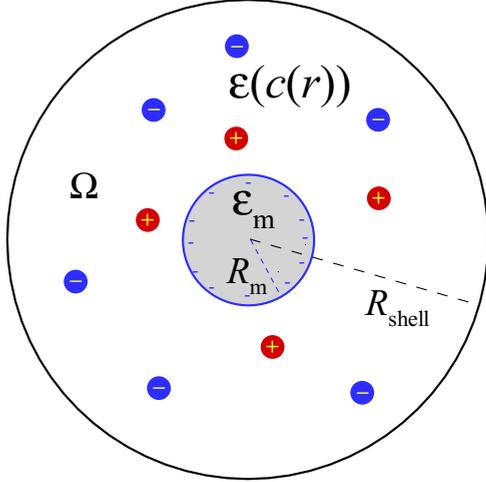
FIG. 1. Schematic representation of a charged colloid immersed in an electrolyte. Cations and anions are represented by solid red and blue balls.

i.e., they only depend on $r = |\mathbf{r}|$. We shall also use the notation $c = c(r) = c(\mathbf{r})$.

We divide our system region into three regions of concentric spherical shells:

(1) The macroion region: $r < R_m$. This region has the constant dielectric coefficient ε_m, same as that of the colloidal particle.

(2) The EDL or electrolyte solution region: $R_m < r < R_{shell}$. In this region, the dielectric coefficient at a spatial point $\mathbf{r}$ is given by $\varepsilon = \varepsilon(c(\mathbf{r})) = \varepsilon(c(r))$, where $c = c(\mathbf{r})$ is the total ionic concentration at $\mathbf{r}$ and $\varepsilon = \varepsilon(c)$ is defined in Eq. (1).

(3) The bulk region: $r > R_{shell}$. In the bulk region far away from the charged interface, the dielectric coefficient is assumed to be a constant $\varepsilon_\infty = \varepsilon(c(\infty))$ where $c(\infty)$ is the bulk value of the total concentration.

Note that all the microions are placed in the region $R_m < r < R_{shell}$.

We define the Hamiltonian $U = U(\mathbf{r}_0, \mathbf{r}_1, \ldots, \mathbf{r}_N)$ of our system to be

$$U = U_{hs} + \sum_{0 \leqslant i < j \leqslant N} U_{ij} + \sum_{i=0}^{N} U_i^{self}, \qquad (2)$$

where the indices i and j run over all macroions and microions with $i = 0$ representing the macroion. Here, the first term U_{hs} is the hard-sphere potential: $U_{hs} = \infty$ if any two ionic spheres (micro or macro) overlap, or the center of any microion goes out of the region of electrolyte solution $R_m < r < R_{shell}$; and $U_{hs} = 0$ otherwise.

The second term in the Hamiltonian (2) sums over the pairwise electrostatic interactions among all different charges, including the macroion which is labeled by 0. We denote $\mathbf{r}_0$ the center of macroion, which is the origin, and $z_0 = Z_0$ and $q_0 = Q_0$. Given i and j with $i \neq j$, the electrostatic interaction U_{ij} between the charges $q_i = z_i e$ and $q_j = z_j e$ located at $\mathbf{r}_i$ and $\mathbf{r}_j$, respectively, can be expressed as $U_{ij} = q_i q_j G(\mathbf{r}_i, \mathbf{r}_j)$. Here, $G(\mathbf{r}, \mathbf{r}')$ is the Green's function defined by

$$-\nabla \cdot \varepsilon(r)\varepsilon_0 \nabla G(\mathbf{r}, \mathbf{r}') = \delta(\mathbf{r} - \mathbf{r}'), \qquad (3)$$

where ε_0 is the vacuum permittivity, δ is the Dirac delta function, and the dielectric coefficient $\varepsilon(r)$ is defined to be ε_m for $r < R_m$, $\varepsilon(c(r))$ for $R_m < r < R_{shell}$, and ε_∞ for $r > R_{shell}$. The Green's function is defined in the entire space $\mathbb{R}^3$. It satisfies that for a fixed $\mathbf{r}'$ both G and $\varepsilon(r)\partial_r G$ are continuous functions with respect to r across the interfaces $r = R_m$ and R_{shell}, and that $G(\mathbf{r}, \mathbf{r}') \to 0$ as $r \to \infty$.

The Green's function $G(\mathbf{r}, \mathbf{r}')$ represents the electrostatic potential due to a unit point charge at $\mathbf{r}'$. It thus describes the electrostatic interaction between two unit charges at $\mathbf{r}$ and $\mathbf{r}'$, respectively. With the radially symmetric dielectric medium, we can decompose the Green's function into

$$G(\mathbf{r}, \mathbf{r}') = G_{Coul}(\mathbf{r}, \mathbf{r}') + G_{Pol}(\mathbf{r}, \mathbf{r}'), \qquad (4)$$

where the term $G_{Coul}(\mathbf{r}, \mathbf{r}')$ is the direct Coulomb interaction term, defined to be

$$G_{Coul}(\mathbf{r}, \mathbf{r}') = \frac{1}{4\pi\varepsilon_0 \sqrt{\varepsilon(r)\varepsilon(r')}|\mathbf{r} - \mathbf{r}'|}, \qquad (5)$$

and the term $G_{Pol}(\mathbf{r}, \mathbf{r}')$ describes the polarization due to both the dielectric jump at the surface of macroion and the dielectric variation in the EDL region. Once $G(\mathbf{r}, \mathbf{r}')$ is known, then it together with (4) and (5) determine $G_{Pol}(\mathbf{r}, \mathbf{r}') = G(\mathbf{r}, \mathbf{r}') - G_{Coul}(\mathbf{r}, \mathbf{r}')$.

The last term in the Hamiltonian (2) sums over all the self-energies that arise due to the dielectrical inhomogeneity of the medium, for which the free energy cost of inserting an ion becomes space dependent [46]. Such a self-energy can be divided into two contributions: (1) the polarization energy due to the global dielectric variation and (2) the Born energy [47] due to the local finite ionic size effect. Thus, the total self-energy of the ith ion is given by

$$U_i^{self} = \frac{q_i^2}{2}\left[G_{Pol}(\mathbf{r}_i, \mathbf{r}_i) + \frac{1}{4\pi\varepsilon(r_i)\varepsilon_0 R_{b,i}} \right], \qquad (6)$$

where $R_{b,i}$ is the Born radius of the ith ion.

B. Harmonic interpolation method

We use the harmonic interpolation method (HIM) [40,48] to solve Eq. (3) for the Green's function $G(\mathbf{r}, \mathbf{r}')$. This method is based on the following observation: if the square root of dielectric coefficient function is harmonic, then the Green's function can be transformed by a change of variable to a new Green's function that is defined with a constant dielectric coefficient. A key idea in the HIM is then to use a piecewise interpolation of the variable dielectric coefficient in Eq. (3) so that the square root of the interpolated dielectric coefficient function is piecewise harmonic.

We divide the radially symmetric simulation region $0 \leqslant r \leqslant R_{shell}$ into small layered shells $I_l = [r_{l-1}, r_l]$ ($l = 1, \ldots, L$) for some L, where $r_0 = 0$, $r_1 = R_m$, and $R_L = R_{shell}$. Let us denote $\varepsilon_j = \varepsilon(r_j)$ the dielectric coefficient at r_j ($j = 0, 1, \ldots, L$). We then approximate the dielectric coefficient function by the following piecewise defined function $\varepsilon_{appr} = \varepsilon_{appr}(r)$: $\varepsilon_{appr} = \varepsilon_m$ if $r_0 \leqslant r \leqslant r_1$, and

$$\varepsilon_{appr}(r) = \varepsilon^l(r)$$

$$= \left(\hat{a}_l + \frac{\hat{b}_l}{r} \right)^2 \quad \text{if} \quad r_{l-1} \leqslant r \leqslant r_l, l = 2, \ldots, L \quad (7)$$

where the coefficients $\hat{a}_l$ and $\hat{b}_l$ are given by

$$\hat{a}_l = \frac{\sqrt{\varepsilon_l}r_l - \sqrt{\varepsilon_{l-1}}r_{l-1}}{r_l - r_{l-1}} \quad \text{and} \quad \hat{b}_l = \frac{\sqrt{\varepsilon_l} - \sqrt{\varepsilon_{l-1}}}{1/r_l - 1/r_{l-1}}.$$

These coefficients are so determined to ensure the continuity of $\varepsilon_{\text{appr}}(r)$.

Now, let $G_{\text{appr}}(\mathbf{r},\mathbf{r}')$ be the Green's function corresponding to $\varepsilon_{\text{appr}}$, i.e., $G_{\text{appr}}(\mathbf{r},\mathbf{r}')$ satisfies Eq. (3) with $\varepsilon(r)$ replaced by $\varepsilon_{\text{appr}}(r)$. We denote $G^l(\mathbf{r},\mathbf{r}') = G_{\text{appr}}(\mathbf{r},\mathbf{r}')$ if $r = |\mathbf{r}| \in I_l = [r_{l-1}, r_l]$. Let the source charge $\mathbf{r}'$ be located in I_k for some $k: 1 \leqslant k \leqslant L$, i.e., $r' = |\mathbf{r}'| \in I_k = [r_{k-1}, r_k]$. Then, we have that [40]

$$-\nabla^2[\sqrt{\varepsilon^l(r)}\varepsilon_0 G^l(\mathbf{r},\mathbf{r}')]$$
$$= \frac{1}{\sqrt{\varepsilon^k(r')}}\delta(\mathbf{r} - \mathbf{r}') \quad \text{if} \quad r_{l-1} < r < r_l, l = 1, \dots, L.$$

Notice that, if we set $v_l = \sqrt{\varepsilon^l}\varepsilon_0 G^l$, then the left-hand side of the above equation on I_l is just $-\nabla^2 v_l$. The equation is then Poisson's equation with a constant dielectric coefficient, in contrast to Eq. (3) that has a variable dielectric coefficient.

We use the spherical coordinates, and denote the angle between $\mathbf{r}$ and $\mathbf{r}'$ by θ. Then, within the layer I_l, the Green's function can be expanded into a series of spherical harmonics

$$4\pi\varepsilon_0 G^l(\mathbf{r},\mathbf{r}') = \frac{1}{\sqrt{\varepsilon^l(r)}} \sum_{n=0}^{\infty}[A_l(n)r^n + B_l(n)r^{-n-1}]P_n(\cos\theta)$$
$$+ \frac{\delta_{lk}}{\sqrt{\varepsilon^l(r)\varepsilon^k(r')}}\frac{1}{|\mathbf{r}-\mathbf{r}'|}, \quad r \in I_l$$

where δ_{lk} is the Kronecker delta and P_n is the Legendre polynomial of order n. Applying the spherical harmonics expansion to the reciprocal distance $1/|\mathbf{r}-\mathbf{r}'|$, we can rewrite the above expression as

$$4\pi\varepsilon_0 G^l(\mathbf{r},\mathbf{r}') = \sum_{n=0}^{\infty} M_{l,n}(r)P_n(\cos\theta), \quad r \in I_l$$

where

$$M_{l,n}(r) = \frac{A_l(n)r^{2n+1} + B_l(n)}{\sqrt{\varepsilon^l(r)}r^{n+1}} + \frac{\delta_{lk}r_<^n}{\sqrt{\varepsilon^l(r)\varepsilon^k(r')}r_>^{n+1}},$$

and $r_<$ ($r_>$) is the smaller (larger) one of r and r'. All the constants $A_l(n)$ and $B_l(n)$ are determined by the following continuities:

$$G^l(\mathbf{r}_l,\mathbf{r}') = G^{l+1}(\mathbf{r}_l,\mathbf{r}'),$$
$$\varepsilon^l(r_l)\frac{\partial G^l(\mathbf{r}_l,\mathbf{r}')}{\partial r} = \varepsilon^{l+1}(r_l)\frac{\partial G^{l+1}(\mathbf{r}_l,\mathbf{r}')}{\partial r}, \quad l = 1, \dots, L-1.$$

The boundedness at the origin of the electrostatic potential leads to $B_1(n) = 0$ for all n. The fact that the potential goes to 0 as $r \to \infty$ leads to $A_L(n) = 0$ for all n. By the orthogonality of the Legendre polynomials, we have

$$M_{l,n}(r_l) = M_{l+1,n}(r_l),$$
$$\varepsilon^l(r_l)\frac{\partial M_{l,n}(r_l)}{\partial r} = \varepsilon^{l+1}(r_l)\frac{\partial M_{l+1,n}(r_l)}{\partial r}, \quad l = 1, \dots, L-1 \quad (8)$$

for all $n = 0, 1 \dots$. For each n, this is a system of $2(L-1)$ linear equations for $2(L-1)$ unknowns, and thus can be solved by direct numerical methods as L is usually a small number.

C. Hybrid Monte Carlo and continuum simulations

We describe our simulations in three steps.

Step 1. Initialization. We input all the parameters: R_{m} and R_{shell} (radii), ε_{m} and ε_{w} (dielectric coefficients), Z_j (valence of an ion of the j ionic species), z_i (valence of the ith ion), a_i and R_{b} (radius and Born radius of the ith ion). (We set $R_{\text{b},i} = a_i$ for all i.) L (number of shells in numerical discretization), r_j ($j = 0, 1, \dots, L$) (grid points), T (temperature), and p (a truncated order in the spherical harmonic expansion). We randomly distribute all the microions without overlap inside the spherical-shell region of electrolyte solution. We also generate an initial guess of the dielectric function $\varepsilon_{\text{init}}$.

Step 2. MC iteration for equilibrating the ionic concentration. This step consists of the following three parts MC1–MC3:

(MC1) Given an approximation of the dielectric coefficient function as defined in (7), we sample a certain number of MC cycles to obtain the ionic concentrations within each discretized radial interval. Each MC cycle is composed of N moves, one for each of the N microions. After each of such a move, we calculate the total energy U and decide to reject or accept the move, all as in a standard MC simulation. Each calculation of the Hamiltonian U involves solving for the Green's function with the HIM. Note that, since only one ion is moved each time, we need only to update part of the total Hamiltonian that is related to the moved ion.

(MC2) Calculate the ionic concentration c_j of the jth ionic species, the total ionic concentration $c = \sum_{j=1}^{M} c_j$, and the dielectric coefficient $\varepsilon = \varepsilon(c(r))$ by Eq. (1). As approximation, each concentration $c_j = c_j(r)$ is assumed to be piecewise constant, i.e., constant value in each of the layers I_l ($l = 1, \dots, L$). This piecewise constant concentration c_j is determined by averaging over snapshots of the microions of the jth ionic species with a certain number of MC cycles, as described in MC1. The resulting dielectric coefficient $\varepsilon = \varepsilon(c(r))$ is also a piecewise constant. In order to improve the HIM accuracy and convergence, we smooth this piecewise dielectric coefficient by fitting it into the following smooth exponential function:

$$\varepsilon(r) = a_1 + a_2 e^{-(r-R_{\text{m}})/\ell_{\text{D}}}, \quad R_{\text{m}} < r < R_{\text{shell}}, \quad (9)$$

where a_1 and a_2 are some fitting constants, and ℓ_{D} is the Debye length defined by $\ell_{\text{D}}^2 = \varepsilon_{\text{w}}\varepsilon_0 k_{\text{B}}T/(\sum_{j=1}^{M} c_j^0 Z_j^2 e^2)$ with c_j^0 the bulk concentration of ions of jth species. Note that we choose the form (9) based mainly on our experience. According to the form (1) of dielectric coefficient function $\varepsilon = \varepsilon(c(r))$, we find that it decays exponentially to the bulk value. Moreover, from the mean-field theory we know that the decay rate should be proportional to the inverse Debye length. Therefore, we construct the function (9). Our numerical tests show that this is a good fitting function in terms of convergence.

(MC3) If the dielectric coefficient function obtained in the previous part does not converge, we then repeat the previous two steps.

Step 3. Data analysis. We use the autocorrelation function (ACF) of the total energy to validate the convergence of sequence of sample energies $E_1, E_2, \ldots, E_K$ for some $K \geqslant 1$. (In our simulations, we choose $K = 10^5$.) The ACF for lag k is defined by

$$\text{ACF}(k) = \frac{1}{K-k} \sum_{i=1}^{K-k} \frac{(E_i - \overline{E})(E_{i+k} - \overline{E})}{\text{var}(E)},$$

where $\text{var}(E)$ and $\overline{E}$ are the variance and the mean of the energies for the K samples, respectively. The ACF reflects how the system decorrelates as a function of MC sampling lags. It also shows the effective number of samples needed for a Markov chain based sampling process. Since we iteratively update the dielectric coefficient function, the ACF also describes the relaxation time of the system in response to the change of dielectric environment. Once the system reaches an equilibrium by MC iterations, we start the MC sampling for the interested physical quantities. These include the macroion-microion radial distribution function (RDF) and the integrated charge distribution function (ICDF). The normalized RDF for the jth ionic species is defined to be $g_j(r) = \widetilde{g}_j(r)/A$, where

$$\widetilde{g}_j(r) = \frac{\langle N_j(r, r + \triangle r) \rangle}{\frac{4}{3}\pi[(r + \triangle r)^3 - r^3]} \quad \text{and}$$

$$A = 4\pi \sum_{j=1}^{M} \int_{R_m}^{R_{\text{shell}}} \widetilde{g}_j(r) r^2 \, dr.$$

The quantity in angular brackets $\langle N_j(r, r + \triangle r) \rangle$ is the average number of ions of the jth species in the spherical shell between r and $r + \triangle r$. The ICDF is defined by

$$Q(r) = Q_0 + \sum_{j=1}^{M} Z_j e \langle N_j(R_m, r) \rangle, \quad R_m \leqslant r \leqslant R_{\text{shell}}.$$

III. A SELF-CONSISTENT CONTINUUM MODEL

We now describe a self-consistent continuum model that includes the effect due to the ionic-concentration-induced variations of dielectric permittivity. We consider an electrolyte solution occupying the spherical shell $R_m < r < R_{\text{shell}}$ as defined in the previous section. We assume again that there are M species of microions in this region. An ion in the jth species has the valence Z_j, and thus carries the charge $Q_j = Z_j e$. We denote by c_j the local concentration of the jth ionic species ($1 \leqslant j \leqslant M$), and by $c = \sum_{j=1}^{M} c_j$ the total ionic concentration. We again assume all these concentrations depend only on $r = |\mathbf{r}|$. We also assume as before that the local dielectric coefficient $\varepsilon = \varepsilon(c(r)) = \varepsilon(c(\mathbf{r}))$ with $\varepsilon(c)$ given by (1) for region $r > R_m$, and a constant value $\varepsilon = \varepsilon_m$ for $r < R_m$.

Let $\Phi = \Phi(r)$ be the electrostatic potential, assumed to be radially symmetric. The following modified Poisson-Boltzmann (PB) equation for the electric potential is the main equation of our self-consistent continuum model [41,49–51]:

$$- \nabla \cdot \varepsilon(c)\varepsilon_0 \nabla \Phi = \sum_{i=1}^{M} Q_i c_i, \tag{10}$$

$$c_i = c_i^0 e^{-\beta(U_i - U_i^b)}, \quad i = 1, \ldots, M. \tag{11}$$

Here, the second equation describes generalized Boltzmann distributions, where c_j^0 is the bulk concentration of the jth ionic species, $\beta = 1/(k_B T)$ is the inverse thermal energy with k_B the Boltzmann constant and T temperature, and for each j ($1 \leqslant j \leqslant M$),

$$U_j = Q_j \Phi + \tfrac{1}{2} Q_j^2 u_j \tag{12}$$

is the electrostatic energy with its bulk value U_j^b [52–55].

In (12), $u_j = u_j(r)$ ($R_m < r < R_{\text{shell}}$) is the self-energy, defined by [46,53,54]

$$u_j(r) = \lim_{\mathbf{r}' \to \mathbf{r}} [G_j(\mathbf{r}, \mathbf{r}') - G_0(\mathbf{r}, \mathbf{r}')], \tag{13}$$

where G_0 is the free-space Green's function defined by

$$-\varepsilon_0 \nabla^2 G_0(\mathbf{r}, \mathbf{r}') = \delta(\mathbf{r} - \mathbf{r}') \tag{14}$$

with $G_0(\mathbf{r}, \mathbf{r}') \to 0$ as $|\mathbf{r} - \mathbf{r}'| \to \infty$, and G_j is the solution to the following generalized Debye-Hückel (DH) equation [56]:

$$- \nabla \cdot \varepsilon_j(\mathbf{r}, \mathbf{r}')\varepsilon_0 \nabla G_j(\mathbf{r}, \mathbf{r}') + 2I_j(\mathbf{r}, \mathbf{r}')G_j(\mathbf{r}, \mathbf{r}') = \delta(\mathbf{r} - \mathbf{r}'), \tag{15}$$

together with the far-field condition $G_j \to 0$ as $|\mathbf{r} - \mathbf{r}'| \to \infty$. In this DH equation, the dielectric coefficient $\varepsilon_j(\mathbf{r}, \mathbf{r}')$ and ionic strength $I_j(\mathbf{r}, \mathbf{r}')$ are determined by

$$\varepsilon_j(\mathbf{r}, \mathbf{r}') = \begin{cases} 1 & \text{if } |\mathbf{r} - \mathbf{r}'| < a_j, \\ \varepsilon_m & \text{if } |\mathbf{r}| < R_m, \\ \varepsilon(c(r)) & \text{otherwise}, \end{cases}$$

$$I_j(\mathbf{r}, \mathbf{r}') = \begin{cases} 0 & \text{if } |\mathbf{r} - \mathbf{r}'| < a_j \text{ or } |\mathbf{r}| < R_m, \\ I(r) = \frac{\beta}{2} \sum_{j=1}^{M} Q_j^2 c_j(r) & \text{otherwise}, \end{cases}$$

where a_j is an effective radius which is taken to be the same as the radius of an ion of the jth species as in our hybrid MC simulations model. Note that, with $\varepsilon_j(\mathbf{r}, \mathbf{r}')$ and $I_j(\mathbf{r}, \mathbf{r}')$ so defined, the self-energy $u_j(r)$, defined in Eq. (13), is a smooth function at every point.

We impose the following boundary conditions for the potential $\Phi = \Phi(r)$:

$$-\varepsilon_m \varepsilon_0 \Phi'(R_m) = \sigma \quad \text{and} \quad \Phi(R_{\text{shell}}) = \Phi_\infty, \tag{16}$$

where $\sigma = Q_0/(4\pi R_m^2)$ with Q_0 the charge at the center (origin) of the macroion as set up in the MC simulations and Φ_∞ is a constant which we usually take it to be 0.

To solve the boundary-value problem of modified PB equations (10) and (16), we need to first solve Eq. (15) to get the functions $G_j(\mathbf{r}, \mathbf{r}')$ ($1 \leqslant j \leqslant M$). Then, we can obtain u_j by (13) and hence U_j from (12) for all j. However, Eq. (15) has variable coefficient and a delta source term, and is hard to solve efficiently in general. Since our purpose is to obtain $u_j(r)$, we generalize the method designed in [41] to decompose u_j into three terms:

$$u_j = u_{j,1} + u_{j,2} + u_{j,3},$$

where

$$u_{j,1}(r) = \lim_{\mathbf{r}' \to \mathbf{r}} [G_j(\mathbf{r}, \mathbf{r}') - G_j'(\mathbf{r}, \mathbf{r}')],$$

$$u_{j,2}(r) = \lim_{\mathbf{r}' \to \mathbf{r}} [G_j'(\mathbf{r}, \mathbf{r}') - G_j''(\mathbf{r}, \mathbf{r}')],$$

$$u_{j,3}(r) = \lim_{\mathbf{r}' \to \mathbf{r}} [G_j''(\mathbf{r}, \mathbf{r}') - G_0(\mathbf{r}, \mathbf{r}')].$$

The functions G'_j and G''_j are defined by

$$-\nabla \cdot \varepsilon'_j(\mathbf{r},\mathbf{r}')\varepsilon_0 \nabla G'_j(\mathbf{r},\mathbf{r}') + 2I_j(\mathbf{r},\mathbf{r}')G'_j(\mathbf{r},\mathbf{r}') = \delta(\mathbf{r} - \mathbf{r}'),$$

$$-\nabla \cdot \varepsilon''_j(\mathbf{r},\mathbf{r}')\varepsilon_0 \nabla G''_j(\mathbf{r},\mathbf{r}') = \delta(\mathbf{r} - \mathbf{r}'),$$

respectively, where

$$\varepsilon'_j(\mathbf{r},\mathbf{r}') = \begin{cases} 1 & \text{if} \quad |\mathbf{r} - \mathbf{r}'| < a_j, \\ \varepsilon(c(r')) & \text{if} \quad |\mathbf{r}| < R_{\mathrm{m}}, \\ \varepsilon(c(r)) & \text{otherwise} \end{cases} \quad \text{and} \quad \varepsilon''_j(\mathbf{r},\mathbf{r}') = \begin{cases} 1 & \text{if} \quad |\mathbf{r} - \mathbf{r}'| < a_j, \\ \varepsilon(c(r')) & \text{otherwise.} \end{cases}$$

We now describe our approximations of $u_{j,k} = u_{j,k}(r)$ ($k = 1,2,3$). By using the method extended from the WKB method developed in [57], we obtain the following approximation of $u_{j,1}$:

$$u_{j,1}(r) \approx \frac{q_{\mathrm{K}}(r)}{4\pi\varepsilon\varepsilon_0|\mathbf{r} - \mathbf{r}_{\mathrm{K}}|} + \int_0^{r_{\mathrm{K}}} \frac{q_{\mathrm{line}}(x)}{4\pi\varepsilon\varepsilon_0|\mathbf{r} - \mathbf{x}|}\,dx, \quad (17)$$

where $\varepsilon = \varepsilon(c(r)), \mathbf{r}_{\mathrm{K}} = \mathbf{r}R_{\mathrm{m}}^2/r^2$, $\mathbf{x} = x\mathbf{r}/r$, and the strengths of the Kelvin and line images are given, respectively, by

$$q_{\mathrm{K}}(r) = -\frac{(\varepsilon_{\mathrm{m}} - \varepsilon)R_{\mathrm{m}}}{(\varepsilon_{\mathrm{m}} + \varepsilon)r}e^{4\pi\varepsilon\varepsilon_0\widetilde{u}|\mathbf{r}-\mathbf{r}_{\mathrm{K}}|},$$

$$q_{\mathrm{line}}(x) = \frac{(\varepsilon_{\mathrm{m}} - \varepsilon)\varepsilon}{(\varepsilon_{\mathrm{m}} + \varepsilon)^2 R_{\mathrm{m}}}\left(\frac{r_{\mathrm{K}}}{x}\right)^{\frac{\varepsilon_{\mathrm{m}}}{\varepsilon_{\mathrm{m}}+\varepsilon}}e^{4\pi\varepsilon\varepsilon_0\widetilde{u}|\mathbf{r}-\mathbf{x}|},$$

with $\widetilde{u}$ defined later in (18). We can use Gauss quadrature to approximate the numerical value of the integral in Eq. (17) as the sum of potentials due to a finite number of image charges [43].

As in [41], we approximate $u_{j,2}$ by

$$u_{j,2}(r) \approx \frac{\widetilde{u}(r)}{1 - 4\pi\varepsilon(c(r))\varepsilon_0\widetilde{u}(r)a_j},$$

where $\widetilde{u}$ does not depend on a_j. It is defined by

$$\widetilde{u}(r) = \lim_{\mathbf{r}'\to\mathbf{r}}[\widetilde{G}'(\mathbf{r},\mathbf{r}') - \widetilde{G}''(\mathbf{r},\mathbf{r}')], \quad (18)$$

where

$$-\nabla \cdot \varepsilon(c(r))\varepsilon_0 \nabla \widetilde{G}'(\mathbf{r},\mathbf{r}') + 2I(r)\widetilde{G}'(\mathbf{r},\mathbf{r}') = \delta(\mathbf{r} - \mathbf{r}'), \quad (19)$$

$$-\nabla \cdot \varepsilon(c(r'))\varepsilon_0 \nabla \widetilde{G}''(\mathbf{r},\mathbf{r}') = \delta(\mathbf{r} - \mathbf{r}'). \quad (20)$$

Note that

$$\widetilde{G}''(\mathbf{r},\mathbf{r}') = \frac{1}{4\pi\varepsilon(c(r'))\varepsilon_0|\mathbf{r} - \mathbf{r}'|}.$$

We use the method developed in [41] to solve for $\widetilde{u}(r)$. Briefly, we introduce $\mathcal{H}(\mathbf{r},\mathbf{r}') = \sqrt{\varepsilon(c(r))\varepsilon(c(r'))}\varepsilon_0\widetilde{G}'(\mathbf{r},\mathbf{r}')$, and transform Eq. (19) into $\nabla^2(\mathcal{H} - \mathcal{H}_0) = v^2\mathcal{H}$, and further into

$$\mathcal{H}(\mathbf{r},\mathbf{r}') - \mathcal{H}_0(\mathbf{r},\mathbf{r}') = -\frac{1}{4\pi}\int \frac{v(\mathbf{r}'')^2\mathcal{H}(\mathbf{r}'',\mathbf{r}')}{|\mathbf{r} - \mathbf{r}''|}\,d\mathbf{r}'',$$

where

$$\mathcal{H}_0(\mathbf{r},\mathbf{r}') = \varepsilon(c(r'))\varepsilon_0\widetilde{G}''(\mathbf{r},\mathbf{r}') = \frac{1}{4\pi|\mathbf{r} - \mathbf{r}'|},$$

$$v(\mathbf{r})^2 = \frac{\varepsilon_0\sqrt{\varepsilon(c(r))}\nabla^2\sqrt{\varepsilon(c(r))} + 2I(r)}{\varepsilon(c(r))\varepsilon_0}.$$

Replacing $\mathcal{H}$ on the left-hand side of the integral equation by $\mathcal{H}^{(n)}$ and that on the right-hand side by $\mathcal{H}^{(n-1)}$, we get an iteration scheme to compute an approximation of $\mathcal{H}$. Finally, we obtain

$$\widetilde{u}(r) = \frac{1}{\varepsilon(c(r))\varepsilon_0}\lim_{\mathbf{r}'\to\mathbf{r}}[\mathcal{H}(\mathbf{r},\mathbf{r}') - \mathcal{H}_0(\mathbf{r},\mathbf{r}')].$$

Direct calculations lead to [41]

$$u_{j,3}(r) = \frac{1}{4\pi a_j\varepsilon_0}\left[\frac{1}{\varepsilon(r)} - 1\right].$$

This is the Born energy.

Our self-consistent continuum model consists of all the equations and boundary conditions (10)–(16). To solve this system of equations, we use a self-consistent iterative algorithm that consists of the following main steps:

Step 1. Initialize the concentrations fields $c_j^{(0)}$ ($j = 1,\ldots,M$) and electrostatic potential $\Phi^{(0)}$. Set $k = 0$.

Step 2. Compute $c^{(k)} = \sum_{j=1}^M c_j^{(k)}$. Compute $\varepsilon(c_r^{(k)})$ by (1). Calculate

$$u_j^{(k)} = u_{j,1}^{(k)} + u_{j,2}^{(k)} + u_{j,3}^{(k)}, \quad j = 1,\ldots,M$$

as described above.

Step 3. Use an iterative scheme to solve the modified PB equation (10), together with the boundary condition (16):

(1) Set $\Phi^{[0]} = \Phi^{(k)}$. Set $l = 0$.

(2) Solve

$$-\nabla \cdot \varepsilon^{[l]}\varepsilon_0\nabla\Phi^{[l+1]} - \gamma^{[l]}\Phi^{[l+1]} = \sum_{i=1}^M Q_i c_i^{[l]} - \gamma^{[l]}\Phi^{[l]},$$

to get $\Phi^{[l+1]}$, where

$$\varepsilon^{[l]} = \varepsilon(c^{[l]}(r)),$$

$$\gamma^{[l]}(r) = \frac{\left|\sum_{i=1}^M Q_i c_i^{[l]}(r)\right|}{|\Phi^{[l]}(r)| + \delta_0},$$

$$c_i^{[l]}(r) = c_i^0 e^{-\beta(U_i^{[l]} - U_i^{\mathrm{b}})},$$

$$U_i^{[l]} = Q_i\Phi^{[l]} + \frac{1}{2}Q_i^2 u_i^{(k)}.$$

Here, $\delta_0 > 0$ is a small number set to ensure the convergence of iteration.

(3) Check if $|\Phi^{[l+1]} - \Phi^{[l]}| < \delta_1$ for some given tolerance δ_1. If not, set $l := l + 1$ and go to (2). If yes, set $k := k + 1$ and $\Phi^{(k)} = \Phi^{[l+1]}$.
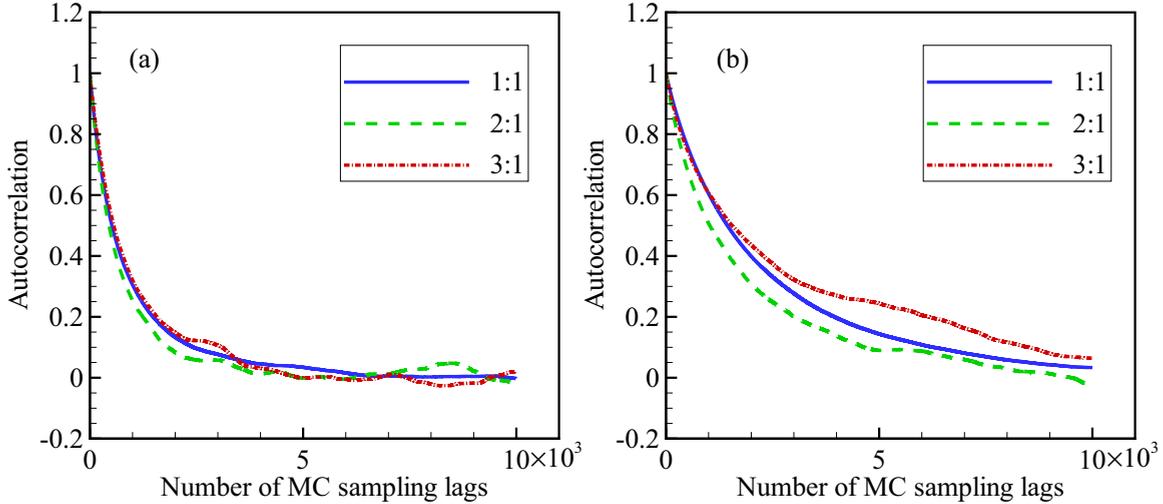
FIG. 2. The autocorrelation function (ACF) with the surface charge density (a) $\sigma = -0.318\ e/\text{nm}^2$ and (b) $\sigma = -1.214\ e/\text{nm}^2$, and with different ionic valences.

Step 4. Compute $c^{(k)} = \sum_{j=1}^{M} c_j^{(k)}$. Compute $\varepsilon(c_r^{(k)})$ by (1). Calculate

$$u_j^{(k)} = u_{j,1}^{(k)} + u_{j,2}^{(k)} + u_{j,3}^{(k)}, \quad j = 1, \ldots, M.$$

Check if $|u_j^{(k)} - u_j^{(k-1)}| < \delta_2$ for all $j = 1, \ldots, M$ for some given tolerance δ_2. If not, go to Step 3.

IV. SIMULATION RESULTS AND DISCUSSIONS

We perform NVT-ensemble Metropolis MC simulations based on the hybrid scheme for the extended primitive model, and study the effect of dielectric variations under different system settings. The following parameters are assumed to be constant throughout the paper: $R_\text{m} = 2$ nm; $R_\text{shell} = 7$ nm and the volume fraction of macroion remains to be the constant $\sim 2.3\%$; all $a_i = a_\text{ion} = 0.225$ nm; $\varepsilon_\text{m} = 2$; $\varepsilon_\text{w} = 80$; $\varepsilon_\text{init} = 80$; $T = 300$ K; and $p = 60$. We choose $p = 60$ based on some numerical tests as well as a rough estimate on the error in the spherical harmonic approximation. The worst case for the convergence of spherical harmonics series is when an ion touches the interface. In this case, the expansion coefficients for the self-energy are about $R_\text{m}^{2n}/(R_\text{m} + a_\text{ion})^{2n}$. In the simulations, we have $R_\text{m} = 2$ nm and $a_\text{ion} = 0.225$ nm. Hence, with $n = 60$, this coefficient is 2.78×10^{-6}. A further estimate on the truncation error for the self-energy leads to at least a five-digit accuracy.

We use $k_\text{B}T$ as the energy unit, where k_B is the Boltzmann constant. We use $1:1$, $2:1$, and $3:1$ salts; so, the coions are always monovalent. We focus on studying the influence of the variance of counterions. In the meantime, we fix the concentration of coions to be 100 mM, allowing a relatively fair comparison. Clearly, the presence of multivalent counterions makes the underlying system strongly correlated. We thus expect that an adequate treatment of electrostatic self-energy is essential. Finally, we choose the macroion surface charge density σ to satisfy that $0 < -\sigma < 3e/\text{nm}^2$, describing many realistic biological and physical systems.

In each of our hybrid MC simulations, we begin with a uniform dielectric coefficient $\varepsilon_\text{init} = \varepsilon_\text{w} = 80$. We then iteratively update the dielectric coefficient function for 50 loops to make sure that we obtain the converged dielectric coefficient function. Each loop consists of 10^3 MC cycles followed by the calculation of the total ionic concentration and the corresponding dielectric coefficient function $\varepsilon(c(r))$. In each cycle, we move all the N microions one by one. Each single move is followed by the calculation of interaction potential U and either acceptance or rejection of this move as described in MC1 in Sec. II C. After the dielectric function reaches convergence, we perform another 10^6 cycles for equilibration of the ionic distribution, and then sample $10^5 N$ cycles for statistics.

A. Convergence analysis

We first analyze numerically the convergence of our iterative scheme. From the first $K = 10^5$ MC samples, we compute the ACF of the total energies. Figure 2 shows the ACFs with surface charge densities (a) $\sigma = -0.318\ e/\text{nm}^2$ and (b) $\sigma = -1.214\ e/\text{nm}^2$, respectively. For each of these two cases, we plot three ACF curves corresponding to three different counterion valences, respectively. For the case of low surface charge [Fig. 2(a)], the ACFs decay to less than 0.2 at about 1500 sampling lags. Furthermore, by comparing the three different curves, we find the ACF for trivalent ions shows the slowest decay. This is reasonable because of the strongest electrostatic coupling in this case, leading to a longer relaxation process for the system to decorrelate. Meanwhile, in the case of higher surface charge [Fig. 2(b)], all the three ACF curves decay to less than 0.2 at more than 3000 sampling lags, and even more than 5000 for the trivalent counterions. Clearly, a stronger surface charge density will lead to a much slower system decorrelation. Finally, the ACF curves help us understand how many numbers of moves are needed within each iteration for updating the dielectric coefficient function. Obviously, more steps are needed for $\sigma = -1.214\ e/\text{nm}^2$ than that for $\sigma = -0.318\ e/\text{nm}^2$, especially when trivalent ions are present.
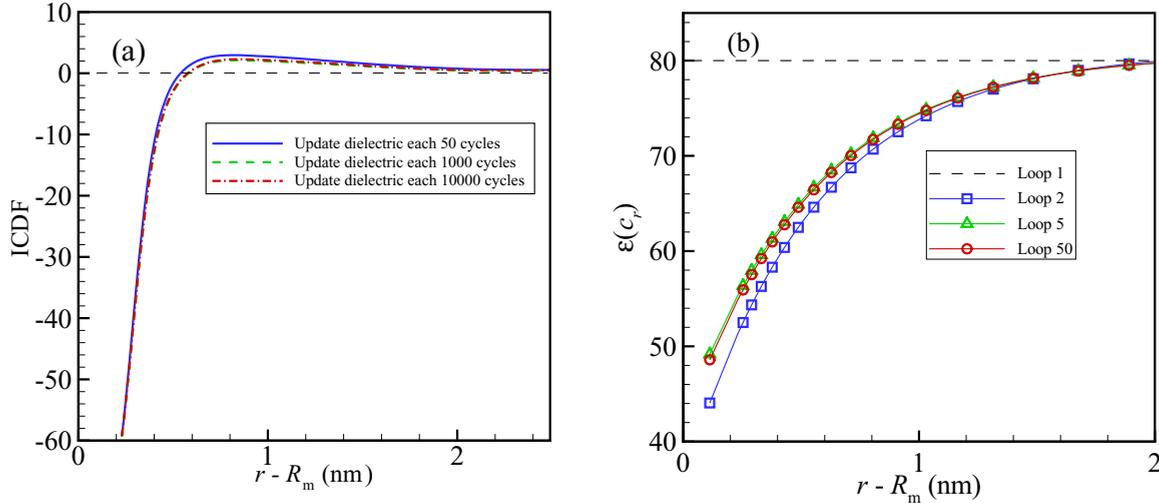
FIG. 3. (a) The integrated charge distribution functions (ICDFs) for three different rates of updating dielectric coefficient function: every 50, 1000, and 10 000 MC cycles. (b) The evolution of dielectric coefficient function at different iteration loops with the dielectric coefficient updated every 1000 MC cycles. Both (a) and (b) are calculated with the surface charge density $\sigma = -1.214\ e/\text{nm}^2$ and with 3:1 electrolyte (trivalent counterions and monovalent coions).

In Fig. 3, we show that too fast updating of the dielectric coefficient function can lead to discrepancy in the final statistical averaging. In Fig. 3(a), we consider the slowest convergence at $\sigma = -1.214\ e/\text{nm}^2$ with trivalent counterions. We compare the final equilibrium integrated charge distribution functions (ICDFs) with respect to the three different rates of updating the dielectric coefficient function: every 50, 1000, and 10 000 MC cycles. Clearly, if we update the dielectric coefficient function every 50 MC cycles, then the resulting ICDF will be different from the other two curves, even the total number of samples is kept the same. In Fig. 3(b), we also present the evolution of the dielectric coefficient function within the iterative process, for the case of updating the dielectrics every 1000 cycles. The dashed line is the initial dielectric coefficient function, which is taken to be a constant. At the second iteration loop, we find that the dielectric coefficient function exhibits a significant change. This is actually already quite close to the final equilibrated dielectric function. Then, in the next loops, the dielectric coefficient function slowly converges.

We remark that, with the adjustment of dielectric function and step size, our Monte Carlo simulation algorithm can be non-Markovian. Convergence and correct description of ergodicity of a non-Markovian algorithm have been partially established in [58]. Our extensive tests have shown that our algorithm indeed converges.

B. Influence of surface charges and multivalent counterions

We now study the effect of concentration-dependent dielectric permittivity $\varepsilon(c(r))$ under the influence of surface charges, with both low and high densities, and counterion multivalences. We also compare our hybrid MC simulations with the standard MC simulations in which the dielectric coefficient in the region of electrolyte is taken to be $\varepsilon_w = 80$. The simulated radial distribution functions (RDFs) are shown in Fig. 4.

We first consider the case of a weakly charged surface with the surface charge density $\sigma = -0.318\ e/\text{nm}^2$. We find the following from the left three plots in Fig. 4: (1) The counterion distribution decreases monotonically in the case of 1:1 salt [Fig. 4 (a)], and become nonmonotonic when the counterions are multivalent [Figs. 4(c) and 4(e)]. This is mainly due to the stronger image charge repulsion that scales quadratically with respect to the counterion valence, resulting a depletion zone and thus the nonmonotonicity. (2) There is a little discrepancy in the RDFs between the case of concentration-dependent dielectric coefficient and that of a constant dielectric coefficient, even when trivalent counterions are present. Such discrepancy indicates that, when the interface is weakly charged, the EDL structure is hardly affected by variations in the local dielectric permittivity. This is mainly due to the relatively small difference of the ionic concentration near the interface compared with the bulk value. It results a dielectric coefficient function without drastic change according to Eq. (1).

We then consider the case of a strongly charged surface with the surface charge density $\sigma = -1.214\ e/\text{nm}^2$. The corresponding RDFs are presented in the three plots of the right column of Fig. 4. We can observe several interesting phenomena: (1) The counterion distribution decreases monotonically for both monovalent and divalent counterions [Figs. 4(b) and 4(d)], and the depletion zone finally appears when trivalent counterions are present [Fig. 4(f)]. Clearly, comparing with the low surface charge density, it becomes harder to form the depletion zone. This is mainly due to the stronger attraction between the surface charges and the counterions. Such attraction overwhelms the image charge repulsion. (2) As shown in Fig. 4(f), even the coion distribution profiles are nonmonotonic, indicating the occurrence of charge inversion. This is also verified in their profiles of integrated charge distribution function (ICDF) shown in Fig. 3(a): the ICDFs change their sign from negative to positive at a certain radial distance. (3) Comparing the counterion RDFs between
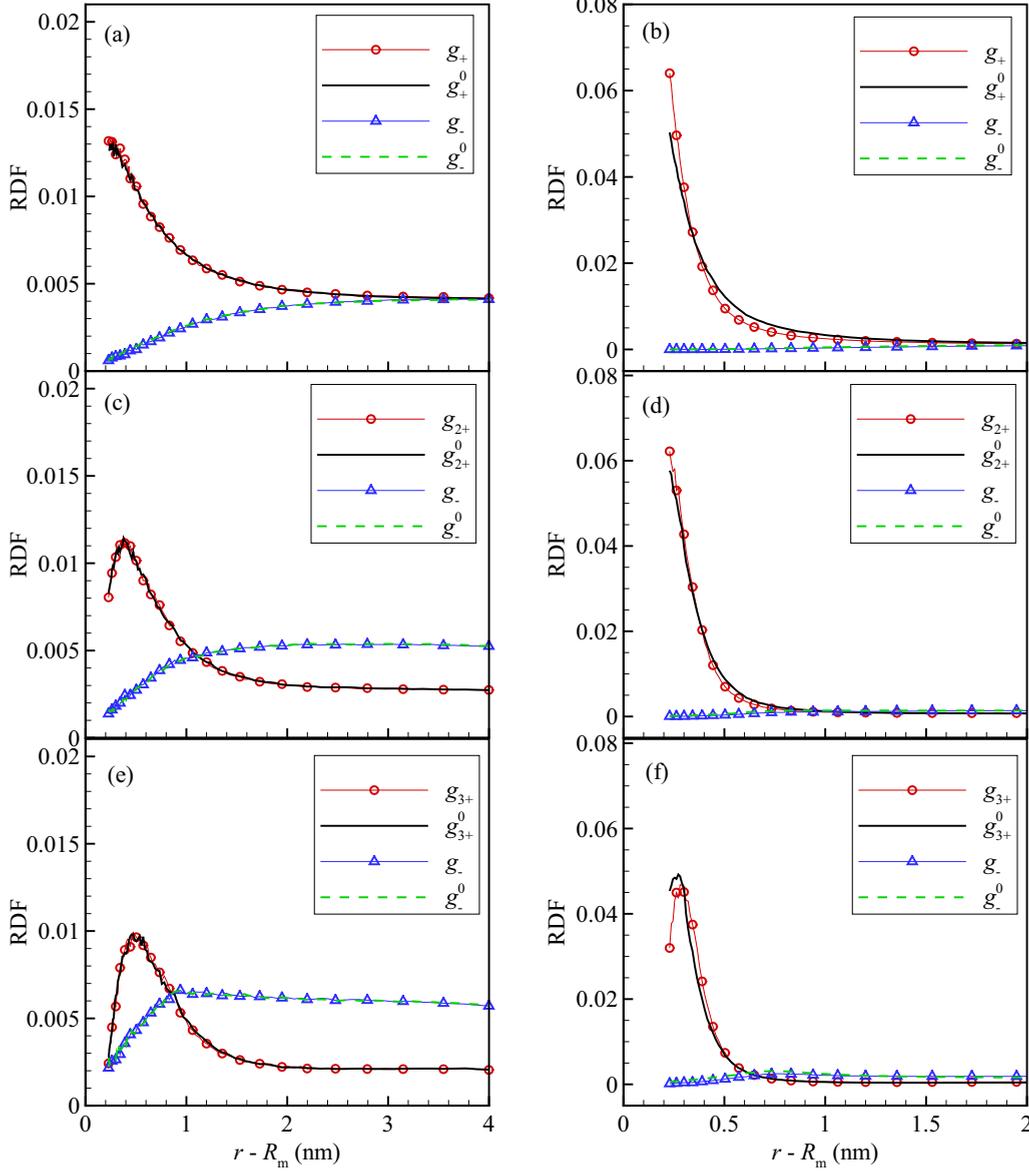
FIG. 4. Counterion and coion radial distribution functions (RDFs) of the distance to the surface of macroion. RDFs for monovalent, divalent, trivalent counterions, and coions with the ionic-concentration-dependent dielectric function $\varepsilon(c(r))$ are denoted by g_+, g_{2+}, g_{3+}, and g_-, respectively. RDFs for monovalent, divalent, trivalent counterions, and coions with a constant dielectric coefficient $\varepsilon = 80$ are denoted by g_+^0, g_{2+}^0, g_{3+}^0, and g_-^0, respectively. The anion concentration is fixed to be 100 mM. (a) 1:1 electrolyte and $\sigma = -0.318\ e/\text{nm}^2$. (b) 1:1 electrolyte and $\sigma = -1.214\ e/\text{nm}^2$. (c) 2:1 electrolyte and $\sigma = -0.318\ e/\text{nm}^2$. (d) 2:1 electrolyte and $\sigma = -1.214\ e/\text{nm}^2$. (e) 3:1 electrolyte and $\sigma = -0.318\ e/\text{nm}^2$. (f) 3:1 electrolyte and $\sigma = -1.214\ e/\text{nm}^2$.

the case of concentration-dependent dielectric coefficient and that of constant dielectric coefficient, we find a very interesting phenomenon: as the counterion valence increases from monovalent to trivalent, the effect of dielectric variation changes from attraction into repulsion. This is mainly due to the complicated interplay between the Born energy and dielectric-boundary-induced repulsion and the correlation-energy-induced attraction. The dielectric-boundary repulsion energy scales as $\sim z^2$ with z being the valence. When the valence is high, this energy cannot be completely screened by the surface charge, and is also enhanced by the Born energy, leading to a stronger depletion interaction.

C. Comparison between hybrid MC simulations and the self-consistent continuum model

We now compare our hybrid MC simulations results with the SCCM calculations as well as the classical PB model. All parameters in the finite difference schemes for the SCCM and PB calculations are consistent with those in MC simulations. Note that if we drop the self-energy term in (11), then we obtain the classical PB model. The computational region $r - R_\text{m}$ is from 0 to 4 nm and is discretized with 1600 grid points in the radial direction.

In Fig. 5, we compare the profiles of cation density (which is the same as anion density) obtained by the MC simulations
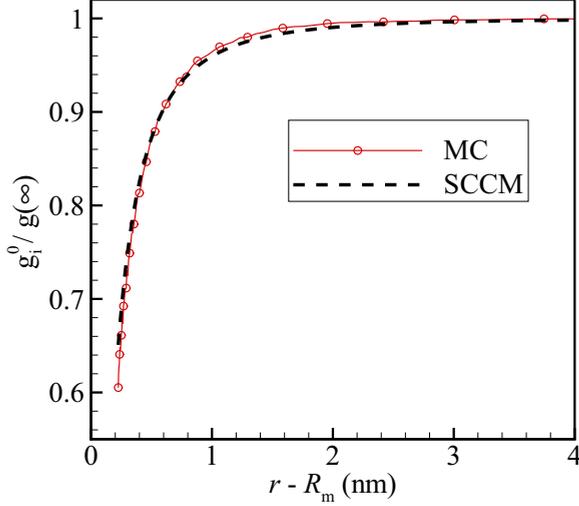
FIG. 5. The comparison of caion (anion) density profiles by MC simulations and SCCM model for a 1:1 dilute electrolyte (13 mM) around a neutral ($\sigma = 0$) macroparticle, where g_i^0 is g_+^0 or g_-^0.

and our SCCM model for a 1:1 dilute electrolyte (13 mM) with $\varepsilon(c(r)) = 80$ around a neutral macroparticle (i.e., the surface charge density $\sigma = 0$). We find that the two profiles are almost the same, indicating that our SCCM can capture the dielectric boundary effect. Note that the PB equation would predict a zero electrostatic potential and hence constant ionic density.

In Fig. 6, the scaled RDFs computed from the self-consistent continuum model (g_i^{CM}) and the classical PB theory (g_i^{PB}) are plotted for two cases: (a) a weakly charged surface with the surface charge density $\sigma = -0.318 \, e/\mathrm{nm}^2$ and 2 : 1 salts; (b) a strongly charged surface with the surface charge density $\sigma = -1.214 \, e/\mathrm{nm}^2$ and 1 : 1 salts. In Fig. 6(a), the results of self-consistent continuum model (SCCM) are in very good agreement with those of the hybrid MC simulations. Note that Fig. 4(c) has already shown that the effect of variable ε is not significant in this case. Thus, the dielectric boundary

effect dominates here and the corresponding approximation technique in Eq. (17) performs excellently. In the classical PB theory where both correlation and dielectric boundary effects are neglected, RDFs are shown to be monotonically decreasing, qualitatively different from what is expected. This indicates that when considering the dielectric boundary effect, classical PB theory fails even when the surface is weakly charged. In Fig. 6(b), with a high surface charge density, the dielectric profile near the surface varies significantly. This affects the accuracy of approximation for $u_{j,2}$ in the SCCM, although the dielectric boundary effect is highly screened by the dense ionic concentrations. This leads to a slight deviation between the RDFs of the self-consistent continuum model and the hybrid MC simulations at the vicinity of the interface. Meanwhile, in the classical PB theory, the RDF of counterions is much larger than both the SCCM and the hybrid MC simulations since it ignores both the Born energy and dielectric boundary effect in $u_{i,1}$, These are in fact crucial in this case.

V. CONCLUSIONS

This work aims at understanding the effect of ionic-concentration-induced dielectric variations to the electric double layer (EDL) structure of an electrolyte solution near a charged surface. Our starting point is the experimentally observed dependence $\varepsilon = \varepsilon(c)$ of the dielectric coefficient ε on the local, total salt ionic concentration c; cf. Eq. (1). This simple relation can be explained as a result of local molecular polarization and inhomogeneous response to an applied field. Yet, the many-body effect arising from such dependence is quite delicate and often significant.

We have constructed a hybrid model combining Monte Carlo (MC) simulations of ions and continuum description of electrostatics. The Hamiltonian of ionic interactions consists of the hard-sphere potential, pairwise charge-charge interactions, and self-energies. Both the second and third parts of this Hamiltonian are defined through Poisson's equation in which the dielectric coefficient varies with the local ionic concentration. This is different significantly from
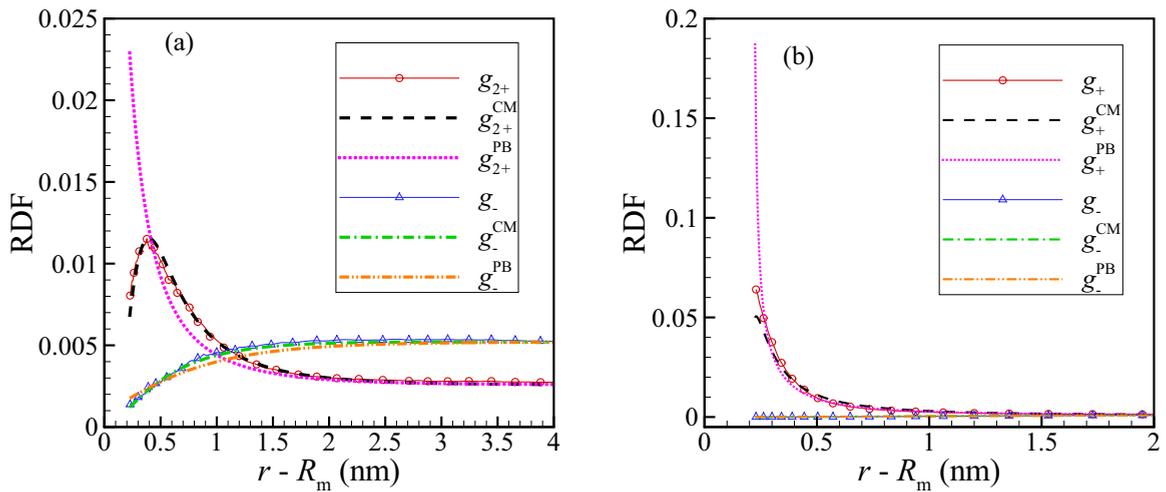

FIG. 6. Counterion and coion radial distribution functions (RDFs) of the distance to the macroion surface from three different models: MC simulations (g_i), self-consistent continuum model (g_i^{CM}), and PB model (g_i^{PB}). Two cases are considered here: (a) a 2 : 1 electrolyte with a low surface charge density $\sigma = -0.318 \, e/\mathrm{nm}^2$ (a); (b) a 1 : 1 electrolyte with a high surface charge density $\sigma = -1.214 \, e/\mathrm{nm}^2$.

the equation with a uniform dielectric coefficient where the interaction potentials have a simple analytic formula. We have implemented the harmonic interpolation method to efficiently solve Poisson's equation within our underlying geometry. We have also developed a self-consistent continuum model in the form of a modified Poisson-Boltzmann (PB) equation that includes various effects, such as the concentration-dependent dielectric variations and self-energy due to the inhomogeneity of dielectric environment. To obtain the self-energy efficiently, we decompose it into different parts that correspond to different dielectric coefficients, and hence different Green's functions. These Green's functions can be obtained by analytical formulas and approximations.

We have verified the convergence of our numerical methods implementing the hybrid MC and continuum model as well as the self-consistent continuum model. By examining the ionic radial distributions and integrated charge distributions with our extensive numerical computations, we have also found that the effect due to the ionic concentration dependence of dielectric permittivity is quite strong if the surface charge density is high. Otherwise, such effect is very small, if the surface is weakly charged. Moreover, with a high surface charge density, the effect is much stronger for a 3:1 than 1:1 electrolyte. In particular, with our hybrid approach, we have captured the depletion of ions near the charged surface and the charge inversion. Our continuum self-consistent model produces results that agree quantitatively with the hybrid MC simulations.

This work is the first step in developing hybrid models and computational methods for complex systems of electrostatic interactions. With several parameters and approximations, our approach is somewhat *ad hoc* and is still in its early stage. While our initial tests have shown that such an approach can capture some of the many-body effects arising from the interplay between the ionic concentration-induced dielectric variations and ion-ion correlations, there is clearly much needed to be improved. First, we have assumed a radially symmetric geometry in our models and methods. This can be limited to many applications that may need a more general geometrical setup. Therefore, extending our approach to general geometries will be of interest. The difficulty in such an extension can be in the construction of efficient numerical

methods for solving for the Green's function, using ideas similar to what have been used in this and previous works. Second, we have included several effects in our models. But, we have not done enough computations to understand which effects are more significant than the others. For instance, it is unclear how important the self-energy is in comparison with the effect due to the ionic-concentration-dependent dielectric variations. Third, we have not taken into account the ionic size effect in our model. Such effects can be quite significant to the EDL structure near a charged surface. It will be interesting then to develop an efficient model to describe such effects [49–51,59], particularly in terms of the ion-ion correlations, and to couple them with other effects in a systematic way. Improved treatments such as a modified fundamental measure theory [60] can be useful for a more accurate description of such correlations. Finally, we have applied different approximate techniques in solving Poisson's or Debye-Hückel equation that define various Green's functions. The accuracy of these numerical methods depends on the smoothness of the dielectric permittivity and ion concentration profiles in electrolytes. Thus, for systems with strong coupling or large gradients in dielectric profiles, we need to develop more robust computational methods.

[1] Y. Levin, Electrostatic corrections: From plasma to biology, Rep. Prog. Phys. **65**, 1577 (2002).

[2] R. H. French, V. A. Parsegian, R. Podgornik, R. F. Rajter, A. Jagota, J. Luo, D. Asthagiri, M. K. Chaudhury, Y.-M. Chiang, S. Granick, S. Kalinin, M. Kardar, R. Kjellander, D. C. Langreth, J. Lewis, S. Lustig, D. Wesolowski, J. S. Wettlaufer, W.-Y. Ching, M. Finnis, F. Houlihan, O. A. von Lilienfeld, C. J. van Oss, and T. Zemb, Long range interactions in nanoscale science, Rev. Mod. Phys. **82**, 1887 (2010).

[3] D. A. Walker, B. Kowalczyk, M. O. de la Cruz, and B. A. Grzybowski, Electrostatics at the nanoscale, Nanoscale **3**, 1316 (2011).

[4] P. Debye and E. Hückel, The theory of electrolytes. I. Lowering of freezing point and related phenomena, Phys. Z. **24**, 185 (1923).

[5] D. L. Chapman, A contribution to the theory of electrocapillarity, Philos. Mag. **25**, 475 (1913).

[6] D. Andelman, Electrostatic properties of membranes: The Poisson-Boltzmann theory, in *Handbook of Biological Physics*, edited by R. Lipowsky and E. Sackmann (Elsevier, Amsterdam, 1995), Vol. 1, pp. 603–642.

[7] J. C. Neu, Wall-Mediated Forces Between Like-Charged Bodies in an Electrolyte, Phys. Rev. Lett. **82**, 1072 (1999).

[8] J. E. Sader and D. Y. C. Chan, Long-range electrostatic attractions between identically charged particles in confined geometries and the Poisson-Boltzmann theory, Langmuir **16**, 324 (2000).

[9] J. E. Sader and D. Y. C. Chan, Long-range electrostatic attractions between identically charged particles in confined

geometries: An unresolved problem, J. Colloid Interface Sci. **213**, 268 (1999).

[10] O. Lenz and C. Holm, Simulation of charge reversal in salty environments: Giant overcharging? Eur. Phys. J. E **26**, 191 (2008).

[11] A. Martin-Molina, J. A. Maroto-Centeno, R. Hidalgo-Alvarez, and M. Quesada-Perez, Testing one component plasma models on colloidal overcharging phenomena, J. Chem. Phys. **125**, 144906 (2006).

[12] A. W. C. Lau, D. B. Lukatsky, P. Pincus, and S. A. Safran, Charge fluctuations and counterion condensation, Phys. Rev. E **65**, 051502 (2002).

[13] D. Ben-Yaakov, D. Andelman, D. Harries, and R. Podgornik, Beyond standard Poisson–Boltzmann theory: Ion-specific interactions in aqueous solutions, J. Phys.: Condens. Matter **21**, 424106 (2009).

[14] D. Ben-Yaakov, D. Andelman, and R. Podgornik, Dielectric decrement as a source of ion-specific effects, J. Chem. Phys. **134**, 074705 (2011).

[15] J. Wen, S. Zhou, Z. Xu, and B. Li, Competitive adsorption and ordered packing of counterions near highly charged surfaces: From mean-field theory to Monte Carlo simulations, Phys. Rev. E **85**, 041406 (2012).

[16] W. G. McMillan and J. E. Mayer, The statistical thermodynamics of multicomponent systems, J. Chem. Phys. **13**, 276 (1945).

[17] P. Linse, Simulation of charged colloids in solution, Adv. Polym. Sci. **185**, 111 (2005).

[18] R. Messina, Image charges in spherical geometry: Application to colloidal systems, J. Chem. Phys. **117**, 11062 (2002).

[19] R. Messina, Electrostatics in soft matter, J. Phys.: Condens. Matter **21**, 113102 (2009).

[20] E. Bichoutskaia, A. L. Boatwright, A. Khachatourian, and A. J. Stace, Electrostatic analysis of the interactions between charged particles of dielectric materials, J. Chem. Phys. **133**, 024105 (2010).

[21] K. Barros and E. Luijten, Dielectric Effects in the Self-Assembly of Binary Colloidal Aggregates, Phys. Rev. Lett. **113**, 017801 (2014).

[22] A. Diehl, A. P. dos Santos, and Y. Levin, Surface tension of an electrolyte-air interface: a Monte Carlo study, J. Phys.: Condens. Matter **24**, 284115 (2012).

[23] D. J. Tobias, A. C. Stern, M. D. Baer, Y. Levin, and C. J. Mundy, Simulation and theory of ions at atmospherically relevant aqueous liquid-air interfaces, Annu. Rev. Phys. Chem. **64**, 339 (2013).

[24] A. van der Vaart, B. D. Bursulaya, C. L. Brooks, and K. M. Merz, Are many-body effects important in protein folding? J. Phys. Chem. B **104**, 9554 (2000).

[25] R. Messina, C. Holm, and K. Kremer, Effect of colloidal charge discretization in the primitive model, Eur. Phys. J. E **4**, 363 (2001).

[26] A. P. dos Santos, A. Bakhshandeh, and Y. Levin, Effects of the dielectric discontinuity on the counterion distribution in a colloidal suspension, J. Chem. Phys. **135**, 044124 (2011).

[27] Z. Gan, X. Xing, and Z. Xu, Effects of image charges, interfacial charge discreteness, and surface roughness on the zeta potential of spherical electric double layers, J. Chem. Phys. **137**, 034708 (2012).

[28] Z. Gan, H. Wu, K. Barros, Z. Xu, and E. Luijten, Comparison of efficient techniques for the simulation of dielectric objects in electrolytes, J. Comput. Phys. **291**, 317 (2015).

[29] D. Boda, D. Gillespie, W. Nonner, D. Henderson, and B. Eisenberg, Computing induced charges in inhomogeneous dielectric media: Application in a Monte Carlo simulation of complex ionic systems, Phys. Rev. E **69**, 046702 (2004).

[30] S. Tyagi, M. Süzen, M. Sega, M. Barbosa, S. S. Kantorovich, and C. Holm, An iterative, fast, linear-scaling method for computing induced charges on arbitrary dielectric boundaries, J. Chem. Phys. **132**, 154112 (2010).

[31] S. Kesselheim, M. Sega, and C. Holm, Applying ICC to DNA translocation: Effect of dielectric boundaries, Comput. Phys. Commun. **182**, 33 (2011).

[32] K. Barros, D. Sinkovits, and E. Luijten, Efficient and accurate simulation of dynamic dielectric objects, J. Chem. Phys. **140**, 064903 (2014).

[33] V. Jadhao, F. J. Solis, and M. O. de la Cruz, Simulation of Charged Systems in Heterogeneous Dielectric Media Via a True Energy Functional, Phys. Rev. Lett. **109**, 223905 (2012).

[34] V. Jadhao, F. J. Solis, and M. O. de la Cruz, A variational formulation of electrostatics in a medium with spatially varying dielectric permittivity, J. Chem. Phys. **138**, 054119 (2013).

[35] F. Fahrenberger, O. A. Hickey, J. Smiatek, and C. Holm, Importance of Varying Permittivity on the Conductivity of Polyelectrolyte Solutions, Phys. Rev. Lett. **115**, 118301 (2015).

[36] J. B. Hasted, D. M. Ritson, and C. H. Collie, Dielectric properties of aqueous ionic solutions. Parts I and II, J. Chem. Phys. **16**, 1 (1948).

[37] A. K. Lyashchenko and A. Y. Zasetsky, Complex dielectric permittivity and relaxation parameters of concentrated aqueous electrolyte solutions in millimeter and centimeter wavelength ranges, J. Mol. Liquids **77**, 61 (1998).

[38] B. Li, J. Wen, and S. Zhou, Mean-field theory and computation of electrostatics with ionic concentration dependent dielectrics, Commun. Math. Sci. **14**, 249 (2016).

[39] N. Gavish and K. Promislow, Dependence of the dielectric constant of electrolyte solutions on ionic concentration: A microfield approach, Phys. Rev. E **94**, 012611 (2016).

[40] F. Fahrenberger, Z. Xu, and C. Holm, Simulation of electric double layers around charged colloids in aqueous solution of variable permittivity, J. Chem. Phys. **141**, 064902 (2014).

[41] M. Ma and Z. Xu, Self-consistent field model for strong electrostatic correlations and inhomogeneous dielectric media, J. Chem. Phys. **141**, 244903 (2014).

[42] M. Ma, S. Zhao, and Z. Xu, Investigation of dielectric decrement and correlation effects on electric double-layer capacitance by self-consistent field model, Commun. Comput. Phys. **20**, 441 (2016).

[43] Z. Xu and W. Cai, Fast analytical methods for macroscopic electrostatic models in biomolecular simulations, SIAM Rev. **53**, 683 (2011).

[44] O. Teschke, G. Ceotto, and E. F. De Souza, Interfacial water dielectric-permittivity-profile measurements using atomic force microscopy, Phys. Rev. E **64**, 011605 (2001).

[45] R. Podgornik, G. Cevc, and B. Žekš, Solvent structure effects in the macroscopic theory of van der Waals forces, J. Chem. Phys. **87**, 5957 (1987).

[46] Z. G. Wang, Fluctuation in electrolyte solutions: The self energy, Phys. Rev. E **81**, 021501 (2010).

[47] M. Born, Volumes and heat of hydratioin of ions, Z. Phys. **1**, 45 (1920).

[48] P. Qin, Z. Xu, W. Cai, and D. Jacobs, Image charge methods for a three-dielectric-layer hybrid solvation model of biomolecules, Commun. Comput. Phys. **6**, 955 (2009).

[49] B. Li, P. Liu, Z. Xu, and S. Zhou, Ionic size effects: Generalized Boltzmann distributions, counterion stratification and modified Debye length, Nonlinearity **26**, 2899 (2013).

[50] B. Li, Continuum electrostatics for ionic solutions with nonuniform ionic sizes, Nonlinearity **22**, 811 (2009).

[51] S. Zhou, Z. Wang, and B. Li, Mean-field description of ionic size effects with non-uniform ionic sizes: A numerical approach, Phys. Rev. E **84**, 021901 (2011).

[52] G. Luo, S. Malkova, J. Yoon, D. G. Schultz, B. Lin, M. Meron, I. Benjamin, P. Vanåk, and M. L. Schlossman, Ion distributions near a liquid-liquid interface, Science **311**, 216 (2006).

[53] R. R. Netz and H. Orland, Variational charge renormalization in charged systems, Eur. Phys. J. E **11**, 301 (2003).

[54] R. R. Netz and H. Orland, Beyond Poisson-Boltzmann: Fluctuation effects and correlation functions, Eur. Phys. J. E **1**, 203 (2000).

[55] B.-S. Lu and X. Xing, Correlation potential of a test ion near a strongly charged plate, Phys. Rev. E **89**, 032305 (2014).

[56] Z. Xu, M. Ma, and P. Liu, Self-energy-modified Poisson-Nernst-Planck equations: WKB approximation and finite-difference approaches, Phys. Rev. E **90**, 013307 (2014).

[57] Frank P. Buff and Frank H. Stillinger, Statistical mechanical theory of double-layer structure and properties, J. Chem. Phys. **39**, 1911 (1963).

[58] H. Haario, E. Saksman, and J. Tamminen, An adaptive Metropolis algorithm, Bernoulli **7**, 223 (2001).

[59] D. Gillespie, A review of steric interactions of ions: Why some theories succeed and others fail to account for ion size, Microfluid. Nanofluid. **18**, 717 (2015).

[60] Y. Rosenfeld, Free-Energy Model for the Inhomogeneous Hard-Sphere Fluid Mixture and Density-Functional Theory of Freezing, Phys. Rev. Lett. **63**, 980 (1989).